Automated Personalised Human Left Ventricular FE Models to Investigate Heart Failure Mechanics

Vicky Y. Wang[1], Corné Hoogendoorn[2], Alejandro F. Frangi[2,3], B.R. Cowan[4], Peter J. Hunter[1], Alistair A. Young[1,4], and Martyn P. Nash[1,5]

[1] Auckland Bioengineering Institute, University of Auckland, New Zealand
{vicky.wang,p.hunter,a.young,martyn.nash}@auckland.ac.nz
[2] Center for Computational Imaging & Simulation Technologies in Biomedicine: Dept. of Info. and Communication Tech., Universitat Pompeu Fabra, Barcelona, Spain
{corne.hoogendoorn,alejandro.frangi}@upf.edu
[3] Department of Mechanical Engineering, University of Sheffield, Sheffield, UK
[4] Centre for Advanced MRI, University of Auckland, New Zealand
b.cowan@auckland.ac.nz
[5] Department of Engineering Science, University of Auckland, New Zealand

Abstract. We have developed finite element modelling techniques to semi-automatically generate personalised biomechanical models of the human left ventricle (LV) based on cardiac magnetic resonance images. Geometric information of the LV throughout the cardiac cycle was derived via semi-automatic segmentation using non-rigid image registration with a pre-segmented image. A reference finite element mechanics model was automatically fitted to the segmented LV endocardial and epicardial surface data at diastasis. Passive and contractile myocardial mechanical properties were then tuned to best match the segmented surface data at end-diastole and end-systole, respectively. Global and regional indices of myocardial mechanics, including muscle fibre stress and extension ratio were then quantified and analysed. This mechanics modelling framework was applied to a healthy human subject and a patient with non-ischaemic heart failure. Comparison of the estimated passive stiffness and maximum activation level between the normal and diseased cases provided some preliminary insight into the changes in myocardial mechanical properties during heart failure. This automated approach enables minimally invasive personalised characterisation of cardiac mechanical function in health and disease. It also has the potential to elucidate the mechanisms of heart failure, and provide new quantitative diagnostic markers and therapeutic strategies for heart failure.

Keywords: Personalised FE modelling, left ventricle, *in vivo* myocardial mechanics, myocardial stiffness, maximum activation level, heart failure.

1 Introduction

Heart failure (HF) is a leading cause of morbidity and mortality with increasing prevalence. Whilst HF symptoms have been conventionally linked with compromised

O. Camara et al. (Eds.): STACOM 2012, LNCS 7746, pp. 307–316, 2013.

pump function (known as systolic HF), it has recently been recognised that equal numbers of patients with HF symptoms appear to have normal systolic function, but impaired diastolic filling, which has been termed diastolic HF. The inter-relationship between diastolic and systolic HF is poorly understood. To investigate changes in ventricular mechanics, personalised heart mechanics models have been used to characterise ventricular mechanical behaviour with the development of advanced cardiac imaging techniques. Such methods typically utilise geometric information of the heart derived from 3D cardiac magnetic resonance images (MRI) to build 3D mechanics models, then use them to estimate myocardial mechanical properties using dynamic MRI. Previous studies have compared healthy and diseased hearts by estimating either the passive tissue stiffness [1] or the myocardial contractility [2][3] in isolation. The primary aim of this study was to develop automated methods for creating personalised biomechanical finite element (FE) models of the heart from 3D cardiac image data and to use these models to estimate tissue stiffness and systolic contractile properties in the same hearts to investigate mechanisms of cardiac dysfunction.

This paper describes the automated fitting of a 3D cardiac mechanics model to human left ventricular (LV) surface data extracted from the Sunnybrook Cardiac database [5]. A semi-automated segmentation method was used to generate ventricular surface data for individual human hearts. The reference LV FE mechanics model was customised to surface data defined at the unloaded state (diastasis) using a nonlinear least squares fitting technique. After incorporating fibre orientations from the Auckland canine heart model [11] and cavity pressure boundary constraints, the LV FE model was used to solve the governing equations for finite deformation continuum mechanics to simulate ventricular deformation throughout the cardiac cycle. Estimations of the diastolic tissue stiffness and systolic contractile properties of the heart were derived by fitting to the geometric data extracted at the end-diastolic (ED) and end-systolic (ES) LV states, respectively. Personalised estimates of the distributions of myocardial fibre extension and stress were also obtained using this modelling framework. We demonstrate this approach using cine magnetic resonance (MR) images from hearts of a healthy human and patient diagnosed with non-ischaemic HF to investigate the underlying mechanisms of dysfunction.

2 Methodology

2.1 Cardiac Images and Segmentation

The LV geometries were extracted using an active shape model (ASM) based approach [6] developed specifically for segmentation of sparse image data. The training set for the statistical shape model was obtained from Computed Tomography studies and comprised shapes of 100 subjects, with 15 shapes per subject sampled throughout the cardiac cycle [7]. The MR image intensity model was obtained from 30 cardiac MR data sets, independent from the Sunnybrook database, after fitting the shape model to their manual segmentations.

The sparse ASM, or SPASM algorithm uses the fact that a 3D image data set is often merely a set of image slices rather than a contiguous 3D volume [8]. It generates shape update steps initially at the intersections of the image slices with the model mesh (the sources), producing update vectors coplanar with the image slices. Through two propagation steps and weighted averaging of update vectors from different sources, this information is 'smeared out' over a larger portion of the model surface. The resulting shape update step thus deforms the shape only near image slices, and consequently is likely to produce implausible shapes. The constraints imposed by the statistical shape model ensure that the resulting shape continues to be a valid LV shape.

Initialisation of the algorithm for the first cardiac phase was done by manual identification of the LV apex and the centroids of the aortic and mitral valves. From these landmarks the initial size and orientation of the model mean mesh were computed. For later cardiac phases, the segmentation of the previous phase was used for initialisation. We constrained the shape model to three standard deviations from the mean in each of its 138 modes.

2.2 Automated Personalisation of the LV Mechanics Model

We adapted an existing canine model with embedded myocardial fibre orientation fields [9], and fitted it to the human LV surface geometry data used in this study.

Data Transformation. The segmented LV surface data were rigidly transformed to a conventional cardiac coordinate system, in which the x-axis is aligned with the long-axis of the LV (passing from the centroid of the LV base through the LV apex); the y-axis is directed from the centroid of the LV to the centroid of the RV (near the mid-ventricle); and the z-axis is oriented in the anterior-to-posterior direction. This transformation procedure was also applied to the ED and ES surface data.

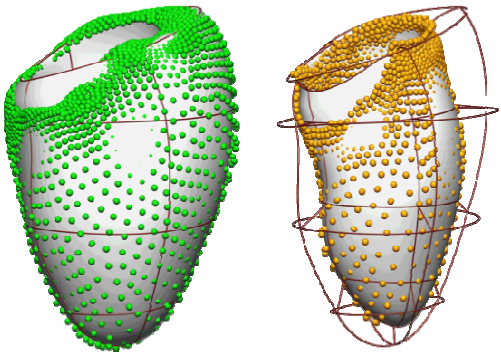

Fig. 1. Personalised LV FE model (brown lines and surfaces) fitted to epicardial (left: green) and endocardial (right: gold) surface points at diastasis of a normal human LV

Geometric Model Creation. We fitted the reference canine FE mechanics model to surface data segmented from the diastasis image using the methods detailed in [10]. Briefly, the FE model consisted of 16 hexahedral finite elements (4 circumferential, 4

longitudinal and 1 radial element) interpolated using C^1 continuous tricubic Hermite basis functions. The human LV surface data were separately projected onto the epicardial and endocardial surfaces of the scaled canine FE model. Nonlinear least-squares optimisation was used to adjust the geometric parameters of each FE model surface to best match the corresponding LV surface data (Fig. 1).

Ventricular Fibre Structure. In order to account for the LV myocardial architecture, we incorporated histologically derived fibre-sheet orientation data from the Auckland canine LV model [9,11]. This choice was primarily due to the lack of detailed *in vivo* or *ex vivo* measurements on human muscle fibre orientation.

Boundary Constraints. LV cavity pressures and displacement boundary constraints were applied during the simulations. The epicardial basal nodes of the model were constrained to match the motion of the segmented surface data, whereas the apex was unconstrained. Due to the lack of *in vivo* cavity pressure data in this study, pressure loading constraints were taken from the literature. During diastolic filling, a LV cavity pressure of 1.48 kPa [12] was applied to the endocardial surface of the reference FE model, whilst the afterload was set to 15.1 kPa [13].

LV Mechanics. LV mechanics was simulated in two phases: 1) passive diastolic filling (slow filling) to ED; and 2) active systolic contraction to ES, which included the isovolumic contraction (IVC) and ejection phases of the cycle. The governing equations of finite deformation elasticity were solved using the FE method.

LV Passive Mechanics and Passive Property Estimation. The passive inflation phase was simulated by incrementally applying pressure to the LV endocardial surface of the model until the preload was reached. The passive mechanical behaviour was modelled using a transversely-isotropic constitutive equation (Eq. 1) [14].

$$W = C_1 \exp(Q)$$
$$\text{where } Q = C_2 E_{ff}^2 + C_3 (E_{cc}^2 + E_{rr}^2 + 2E_{cr}^2) + 2C_4 (E_{fc} E_{cf} + E_{fr} E_{rf}) \quad (1)$$

where $E_{\alpha\beta}$ are the components of Green's (Lagrange) strain tensor referred to fibre (f), cross-fibre (c) and radial (r) material coordinates, and C_1 - C_4 are the passive myocardial constitutive parameters. An estimate of the tissue stiffness (C_1) was obtained after matching the inflated FE mechanics model to the segmented ED surface data. During this optimisation, the segmented data were projected onto their corresponding FE model surfaces, and the overall root-mean-squared error of the projections was then minimised by varying C_1. Other parameters describing the anisotropy (C_2 - C_4) were not included in the estimation due to the lack of regional strain information in the segmented data. Instead, their values were taken from our previous study based on MR tagging in canine hearts [9].

LV Systolic Mechanics and Active Property Estimation. After tuning the passive properties, the simulation was continued through IVC, to the end of ejection. Contraction of the LV model was driven by a calcium-dependent activation transient (T_{Ca}) throughout systole as part of a steady-state model for contractile stress (T_a) [15]:

$$T_a = T_{Ca}\left(1+\beta(\lambda-1)\right) \tag{2}$$

where λ is the fibre extension ratio and β is a material parameter that describes the length-dependence of the activation level. Note that this model is independent of the velocity of muscle shortening. Following the end of inflation, the activation level, T_{Ca}, was gradually increased to represent the release of calcium from the sarcoplasmic reticulum. During IVC, the LV cavity pressure was raised to counteract the contractile force in order to hold the cavity volume constant at its ED value. Simulations ran until the LV cavity pressure reached an afterload of 15.1 kPa [13]. The maximum activation level at ES (T_{Ca_max}) was estimated by matching the model predicted ES state to the segmented human ES data.

3 Results

Fig. 2 illustrates the segmented ED (top) and ES (bottom) epicardial (green) and endocardial (gold) surface points derived from the automatic segmentation procedure described in section 2.1. Global geometric and functional measurements, such as wall volume, EDV, ESV and ejection fraction (EF) were calculated from geometric models fitted to the surface contours at ED and ES. These indices are summarised in Table 1.

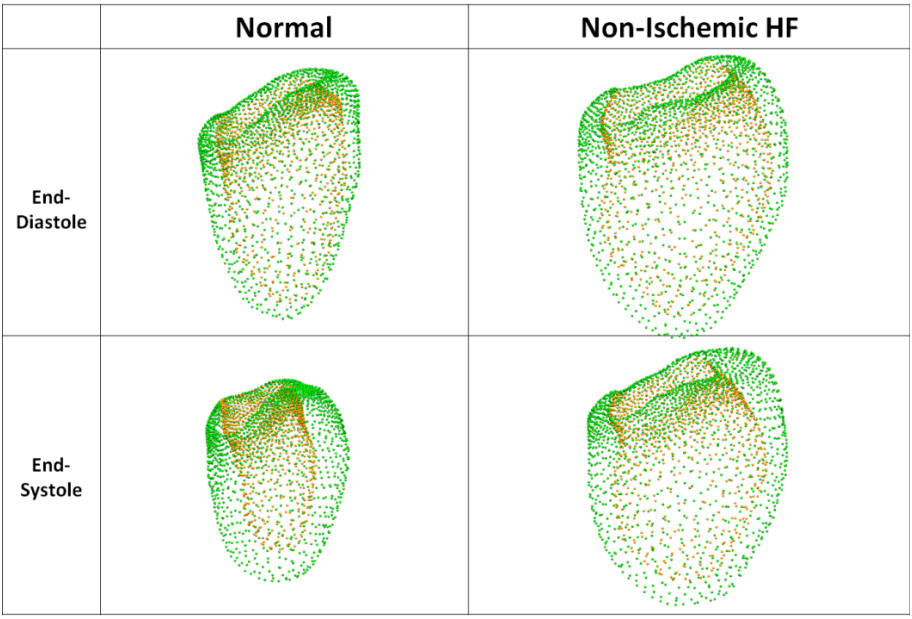

Fig. 2. Epicardial (green) and endocardial (gold) surface points at end-diastole (top) and end-systole (bottom) for LVs from a normal human (left) and non-ischaemic HF patient (right)

For the two cases studied in this paper, both the wall volume and the EDV for the non-ischaemic HF case were approximately double the values for the normal, indicating severe remodelling of the LV geometry with both wall thickening and

ventricular dilatation. The non-ischaemic HF case also exhibited a larger ESV compared to the normal, but the stroke volumes between the two cases were only moderately different (81ml versus 62 ml). The significant reduction in EF seen in the non-ischaemic HF case was primarily due to its increased EDV. Fig. 3 shows the error projections of the segmented data at ED and ES onto the corresponding surfaces of the associated predicted models.

The estimated passive tissue stiffness parameter (C_1) was substantially larger for the non-ischaemic case (Table 2). In contrast, estimated values of the maximum activation level (T_{Ca_max}) were relatively similar. As indicated in Fig. 4, fibre extent of shortening was lower for the non-ischaemic HF case compared to the normal case. This resulted in an increased active fibre stress (T_a) at ES, due to its dependence upon length (the Frank-Starling mechanism), even though the estimated activation levels (T_{Ca}) were similar for the two cases.

Table 1. Geometric and functional data for normal and non-ischaemic heart failure LVs

	Normal	Non-ischaemic Heart Failure
Wall Volume (ml)	105	194
EDV (ml)	119	247
ESV (ml)	38	185
EF (%)	68	25

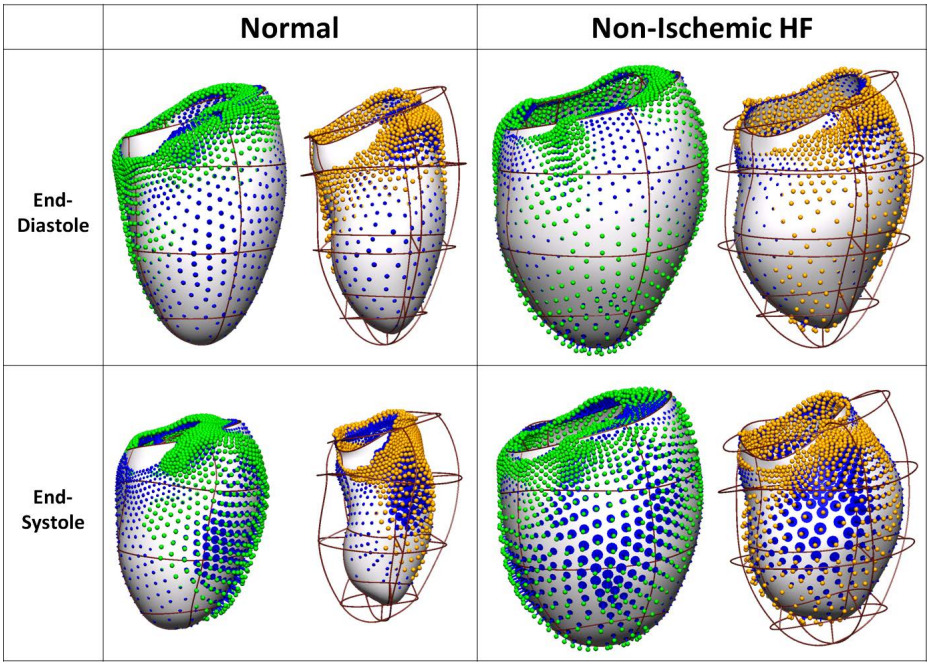

Fig. 3. Predicted ED FE models following passive parameter estimation (upper), and ES models following active contractile parameter estimation (lower). Epicardial (green) and endocardial (gold) surface data error projections (blue) are shown for a normal human LV (left), and a LV of a non-ischaemic heart failure patient (right).

Table 2. Estimated passive and active mechanical properties for normal and non-ischaemic heart failure LVs

	Normal	Non-ischaemic HF
Passive Stiffness (C_1 *(kPa)*)	2.3	7.6
ED Fibre Extension Ratio (λ)	1.1 ± 0.03	1.04 ± 0.02*
ED Passive Fibre Stress *(kPa)*	4 ± 1.9	4 ± 2.6
Maximum Activation Level (T_{Ca_max} *(kPa)*)	93	94
ES Fibre Extension Ratio (λ)	0.89 ± 0.07	0.95 ± 0.07*
ES Active Fibre Stress *(kPa)*	70 ± 14	81 ± 13*

* indicates significant difference (P<0.05) compared to the normal case.

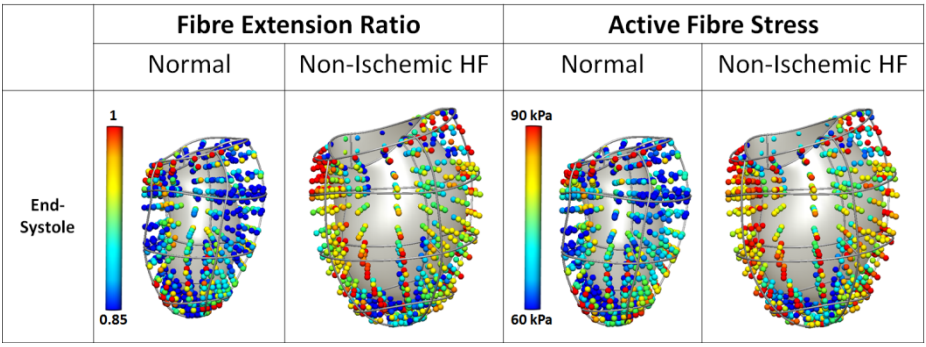

Fig. 4. FE model predictions of end-systolic fibre extension ratio and active fibre stress for two case studies

4 Discussion

This paper presents a workflow to construct LV surface segmentations from cardiac MR images, and to create personalised FE biomechanical models to characterise global mechanical properties of the LV. Although a manual step was required to start the segmentation process by identifying a small number of landmarks, the automatic detection of landmarks is currently feasible and could be applied to produce a fully automated method. These models were used to generate personalised estimates of passive and active mechanical properties by matching model predictions to the kinematic information derived from the cardiac MR images. These methods not only provided estimates of global mechanical function, but also estimates of regional fibre stretch and stress.

A key limitation of this study was the lack of subject-specific cavity pressure measurements, which were not recorded. Therefore, we assumed the same diastolic (preload) and systolic (afterload) blood pressures for both the normal and HF cases. Estimated mechanical properties were shown to be correlated with preload and afterload (data not shown). Lack of pressure transient measurements also limited our mechanical analysis to consider only two time-points for both phases of the cardiac

cycle. If personalised pressure recordings were available, these data could be readily incorporated into this workflow to provide estimates of the activation level transients throughout the cardiac cycle.

A second limitation was the lack of subject-specific microstructural information for the human hearts studied. This may have been particularly limiting for the analysis of the failing hearts. *In vivo* imaging of the myofibre architecture may be made possible using *in vivo* diffusion tensor MR imaging (DTMRI) techniques. Recent attempts to acquire *in vivo* DTMRI of beating heart include [16][17], however the data collected are still rather sparse and the techniques require extensive validation before *in vivo* DTMRI becomes a clinical routine. This framework is capable of incorporating *in vivo* fibre orientation data should they be available in future studies. In [18], statistical atlases of human myocardial fibre orientations for both healthy and abnormal hearts were proposed based on *ex vivo* DTMR imaging of 10 healthy and 6 abnormal hearts. Incorporating the data from this atlas into this modelling framework was beyond the scope of the present study, partly because the physical conditions of these hearts remain unclear. However, in a separate study we are presently underway to investigate the sensitivity of strain predictions on the underlying fibre structure [19] by embedding the fibre data extracted from normal human hearts [18] into the LV mechanics model.

For this paper, we focused on only the LV. The next stage of this study is to extend the analysis to consider both ventricles, and this inclusion can potentially improve the RMSE during parameter estimation.

We tuned the mechanical properties to match the shapes of the LV at ED and ES, and assumed that the distributions of these properties were homogeneous. This assumption may be violated for diseased cases where tissue remodelling (e.g. due to myocardial infarction) may induce regional variation of mechanical properties. However, this choice was made solely due to the lack of regional motion data because the 3D MR images used in this study only allowed derivation of surface information of the LV. To incorporate heterogeneity, regional kinematic data are required. This framework could be readily extended to estimate material parameters on a regional basis.

By applying this automated method to LV images from a normal heart, and the LV of a non-ischaemic HF patient, we were able to compare the estimated mechanical properties. For this study, we focused on the effects of geometric remodelling during HF on mechanical properties estimates. Using this modelling workflow, the estimated passive tissue stiffness for the LV with non-ischaemic HF was greater than that for the normal LV. This is consistent with the fibrosis that is known to occur during HF [12]. The estimated maximum activation levels (T_{Ca_max}) were similar for the two cases, suggesting that non-ischaemic HF is not associated with a change in the systolic mechanical properties of the myocardium. In this study, the geometric remodelling as a result of non-ischaemic HF was fully accounted for by an increase in passive stiffness. We speculate that the increased active fibre stress (T_a) for the non-ischaemic HF case may be responsible for triggering myocardial tissue and chamber remodelling.

5 Conclusions

We have developed an automated segmentation and FE modelling workflow to generate personalised human LV mechanics models using geometric and kinematic information derived from semi-automatic segmentation of cardiac images. The methods presented will be used in a larger-scale study to generate personalised FE mechanics models, and extract patient-specific mechanical properties of hearts from patients with HF. Determining more specific variations in mechanical properties between diseased and normal human hearts will help in the understanding of the underlying mechanisms of HF.

Acknowledgements. This work is funded by the European Commission's Ricordo project (FP7-ICT-248502), within the 7th Framework Programme. CH and AFF have been partially funded by the Industrial and Technological Development Center (CDTI) CENIT-cvREMOD program, by the Spanish Ministry Science and Innovation under grant STIMATH (TIN2009-14536-C02-01), and by the European Commission's project euHeart (FP7-ICT-224495).

References

1. Xi, J., Lamata, P., Shi, W., Niederer, S., Land, S., Rueckert, D., Duckett, S.G., Shetty, A.K., Rinaldi, C.A., Razavi, R., Smith, N.: An Automatic Data Assimilation Framework for Patient-Specific Myocardial Mechanical Parameter Estimation. In: Metaxas, D.N., Axel, L. (eds.) FIMH 2011. LNCS, vol. 6666, pp. 392–400. Springer, Heidelberg (2011)
2. Imperiale, A., Chabiniok, R., Moireau, P., Chapelle, D.: Constitutive Parameter Estimation Methodology Using Tagged-MRI Data. In: Metaxas, D.N., Axel, L. (eds.) FIMH 2011. LNCS, vol. 6666, pp. 409–417. Springer, Heidelberg (2011)
3. Chabiniok, R., Moireau, P., Lesault, P.-F., Rahmouni, A., Deux, J.-F., Chapelle, D.: Trials on Tissue Contractility Estimation from Cardiac Cine MRI Using a Biomechanical Heart Model. In: Metaxas, D.N., Axel, L. (eds.) FIMH 2011. LNCS, vol. 6666, pp. 304–312. Springer, Heidelberg (2011)
4. Sermesant, M., Billet, F., Chabiniok, R., Mansi, T., Chinchapatnam, P., Moireau, P., Peyrat, J.-M., Rhode, K., Ginks, M., Lambiase, P., Arridge, S., Delingette, H., Sorine, M., Rinaldi, C.A., Chapelle, D., Razavi, R., Ayache, N.: Personalised Electromechanical Model of the Heart for the Prediction of the Acute Effects of Cardiac Resynchronisation Therapy. In: Ayache, N., Delingette, H., Sermesant, M. (eds.) FIMH 2009. LNCS, vol. 5528,
pp. 239–248. Springer, Heidelberg (2009)
5. Radau, P., Lu, Y., Connelly, K., Paul, G., Dick, A.J., Wright, G.A.: Evaluation Framework for Algorithms Segmenting Short Axis Cardiac MRI. The MIDAS Journal - Cardiac MR Left Ventricle Segmentation Challenge, `http://hdl.handle.net/10380/3070`
6. Cootes, T.F., Taylor, C.J., Cooper, D.H., Graham, J.: Active shape models - their training and application. Comput. Vis. Image Underst. 61(1), 8–59 (1995)
7. Ordás, S., Oubel, E., Leta, R., Carrera, F., Frangi, A.F.: A statistical shape model of the heart and its application to model-based segmentation. In: Proc. SPIE Medical Imaging, article no. 65111K (2004)

8. van Assen, H.C., Danilouchkine, M.G., Frangi, A.F., Ordás, S., Westenberg, J.J.M., Reiber, J.H.C., Lelieveldt, B.P.F.: SPASM: A 3-D ASM for segmentation of sparse and arbitrarily oriented cardiac MRI data. Med. Imag. Anal. 10(2), 286–303 (2006)
9. Wang, V.Y.: Modelling In Vivo Cardiac Mechanics using MRI and FEM. PhD thesis. The University of Auckland, New Zealand (2011)
10. Wang, V.Y., Lam, H.I., Ennis, D.B., Cowan, B.R., Young, A.A., Nash, M.P.: Modelling passive diastolic mechanics with quantitative MRI of cardiac structure and function. Med. Imag. Anal. 13(5), 773–784 (2009)
11. Nielsen, P.M.F., Le Grice, I.J., Smaill, B.H., Hunter, P.J.: Mathematical model of geometry and fibrous structure of the heart. Am. J. Physiol. 260(4), H1365–H1378 (1991)
12. Honda, H., Nakaya, S., Kamada, H., Hasegawa, H., Demachi, J., Chikama, H., Sugimura, K., Yamamoto, Y., Kumasaka, N., Takita, T., Ikeda, J., Kanai, H., Koiwa, Y., Shirato, K.: Non-invasive estimation of human left ventricular end-diastolic pressure. Med. Eng. Phys. 6, 485–488 (1998)
13. McKay, R.G., Aroesty, J.M., Heller, G.V., Royal, H.D., Warren, S.E., Grossman, W.: Assessment of the end-systolic pressure-volume relationship in human beings with the use of a time-varying elastance model. Circ. 74, 97–104 (1986)
14. Guccione, J.M., McCulloch, A.D., Waldman, L.K.: Passive material properties of intact ventricular myocardium determined from a cylindrical model. J. Biomech. Eng. 113, 43–55 (1991)
15. Hunter, P.J., McCulloch, A.D., ter Keurs, H.E.D.J.: Modelling the mechanical properties of cardiac muscle. Prog. Biophys. Mol. Bio. 69, 289–331 (1998)
16. Dou, J., Tseng, W.I., Reese, T.G., Wedeen, V.J.: Combined diffusion and strain MRI reveals structure and function of human myocardial laminar sheets in vivo. Magnet. Reson. Med. 50(1), 107–113 (2003)
17. Toussaint, N., Sermesant, M., Stoeck, C.T., Kozerke, S., Batchelor, P.G.: *In vivo* Human 3D Cardiac Fibre Architecture: Reconstruction Using Curvilinear Interpolation of Diffusion Tensor Images. In: Jiang, T., Navab, N., Pluim, J.P.W., Viergever, M.A. (eds.) MICCAI 2010, Part I. LNCS, vol. 6361, pp. 418–425. Springer, Heidelberg (2010)
18. Lombaert, H., Peyrat, J.-M., Fanton, L., Cheriet, F., Delingette, H., Ayache, N., Clarysse, P., Magnin, I., Croisille, P.: Statistical Atlas of Human Cardiac Fibers: Comparison with Abnormal Hearts. In: Camara, O., Konukoglu, E., Pop, M., Rhode, K., Sermesant, M., Young, A. (eds.) STACOM 2011. LNCS, vol. 7085, pp. 207–213. Springer, Heidelberg (2012)
19. Wang, V.Y., Casta, C., Croisille, P., Clarysse, P., Zhu, Y.M., Cowan, B.R., Young, A.A., Nash, M.P.: Estimation of in vivo human myocardial fibre strain by integrating diffusion tensor and tagged MRI using FE modelling. In: 9th IEEE International Symposium on Biomedical Imaging (ISBI), pp. 46–49 (2012)